Title:

Prediction of Wood Fiber Attributes from LiDAR-derived Forest Canopy Indicators

Authors:

Hilker, T., G.W. Frazer, N.C. Coops, M.A. Wulder, M. van Leeuwen, G.J. Newnham, D.S. Culvenor, J.D. Stewart

Affiliations:

Thomas Hilker, NASA Goddard Space Flight Center, Biospheric Sciences Branch Code 614.4, Bldg 33, #G310, 8800 Greenbelt Road, Greenbelt, MD 20771—Phone: (301) 286-8597; Fax: (301) 614-6695; ~~thomas.hilker@nasa.gov.~~ thomas.hilker@oregonstate.edu

Gordon W. Frazer, Canadian Forest Service, Natural Resources Canada.

Nicholas C. Coops, University of British Columbia.

Michael A. Wulder, Canadian Forest Service, Natural Resources Canada.

Glenn J. Newnham, CSIRO Land and Water.

James D. Stewart, Canadian Wood Fiber Center, Natural Resources Canada.

Martin van Leeuwen, University of British Columbia.

Darius S. Culvenor, CSIRO Land and Water.

Keywords: LiDAR, wood fiber, canopy structure, light regime, lodgepole pine

ABSTRACT

We investigate the potential use of airborne LiDAR data to predict key wood fiber properties from extrinsic indicators in lodgepole-pine-leading forest stands located in the foothills of central Alberta, Canada. Six wood fiber attributes (wood density, cell perimeter, cell coarseness, mature fiber length, microfibril angle, and modulus of elasticity) were measured at twenty-one plots, and using data reduction techniques, two components of wood properties were derived: (i) wood strength, stiffness and fiber yield (ii) fiber strength and smoothness. These wood fiber components were then compared to extrinsic indicators of wood characteristics derived LiDAR estimated topographic morphology, tree height, and canopy light metrics. The first principal component indicating wood strength, and stiffness was significantly correlated to the depth of different canopy zones (or light regimes) ($r^2 = 0.55$, $p < 0.05$). The second component, related to fiber strength and smoothness was significantly correlated to the height of the canopy and canopy thickness ($r^2 = 0.65$, $p < 0.05$). The results indicate that airborne LiDAR attributes can explain about half of the observed variance in intrinsic wood fiber attributes which is approximately 5 – 10 % less than that explained by growth-related field measured variables such as diameter increment and height. This reduction in explained variance can be balanced by the opportunities for much broader spatial characterizations of wood quantity and quality at the stand and landscape level.

INTRODUCTION

Wood and fiber properties of timber are of paramount importance to foresters, mill operators, and consumers. Differences in wood and fiber properties can impact decisions along the entire value chain, because the economic value of saw logs is largely affected by the properties of wood fiber, log shape and curvature, and number and diameter of branches; pulping quality is largely determined by the fiber length, strength and dimensions. Consequently, information on the quality of standing timber prior to harvest is of enormous benefit to the forestry sector to help optimize harvesting and marketing strategies (Zobel and Van Buijtenen, 1989) and the effective and sustainable management of our forest resources can be optimized using accurate information on wood properties. In addition, wood and fiber attributes also impact biodiversity, carbon sequestration, hydrology, nutrient cycles, and regulation of other key ecological processes. For example, the chemical and physical composition of snags and coarse woody debris will influence the rate of decay and longevity of these structures, and therefore the long-term supply of habitat, substrate, fuels, and nutrients (Spies et al., 1988).

A large number of factors drive wood and fiber properties. At the broadest scale, climate, topography and soils all directly impact the physical and chemical characteristics of timber, most specifically through either the occurrence of different species and site characteristics (Wilhelmsson et al. 2002; Väisänen et al. 1989) or by regulating light absorption and photosynthesis and thus impacting growth. At the stand level, wood fiber properties vary according to stand development, with local topography, wind exposure, moisture and nutrient availability, stocking density, species composition, and disturbance all being linked to wood properties (Downes and Drew, 2008; Kint et al. 2010). At the tree level, the individual growth rate, knot size, type and placement, crown development, crown size and branch placement vary significantly across a range of species and sites (Mansfield et al. 2007; Mäkinen and Colin, 1998).

Van Leeuwen et al. (2011) proposed that wood fiber characteristics can be derived through measurement of either intrinsic or extrinsic indicators of wood properties. Intrinsic indicators relate to the internal, anatomical structure of the wood, the proportions of juvenile and mature wood, as well as the sub-cellular structure, including cell perimeter, length and thickness and microfibril angle (Chen and Evans, 2005; Chen and Evans, 2010). These cellular attributes have recently been measured in radial and

tangential planes using a combination of microscopic digital imagery, X-ray densitometry, and X-ray diffraction (Downes et al. 2002; Downes and Drew, 2008; Evans et al. 2000; Evans and Ilic, 2001).

Information on intrinsic indicators of fiber properties is critical for mill operators and end users; however, such detailed measurements are not generally available over large forest estates prior to harvesting. Extrinsic indicators of wood properties relate to the external characteristics of a tree, including tree height, diameter, stem taper, and crown structure. To assess wood fiber characteristics from standing trees, studies have explored relationships between intrinsic and extrinsic characteristics (Donaldson, 2008; Eriksson et al. 2006). For example Donaldson (2008) undertook detailed work relating wood fiber attributes to tree structure and form (principally height), concluding that height and mechanical stresses on the bole, such as wind and gravity, can all directly impact wood fiber attributes, and thus serve as reliable indicators of wood properties.

Light detection and ranging (LiDAR), has increasingly been used to measure canopy and individual bole and crown characteristics more easily and effectively than standard forestry inventory practices (Coops et al. 2007, Wulder et al 2008). LiDAR systems provide 3-D measures of the forest canopy structure using laser ranging from a known platform location. In forestry, LiDAR is commonly acquired from aircraft or helicopters to support operational and strategic forest resource monitoring and inventory at local or regional scales (Holmgren and Persson, 2004). Airborne LiDAR systems usually record multiple (1 to 5 returns per emitted pulse) discrete-return laser pulses (with a footprint size of 0.1 – 2 m), using the time a laser beam travels between emitting source and reflected target to estimate its distance (Blair et al. 1999). Studies have demonstrated that the LiDAR measurement error for individual tree heights (of a given species) is typically less than 1.0 m (Persson et al. 2002), and less than 0.5 m for plot-based estimates of maximum and mean stand height with full canopy closure (Næsset, 1997; Magnussen and Boudewyn, 1998; Magnussen et al. 1999; Næsset and Økland, 2002; Næsset, 2002). Furthermore, LiDAR estimates of tree and stand height have been shown to be more consistent than field based measurements (Næsset and Økland, 2002).

In this study, we investigate the potential of airborne LiDAR to derive a range of forest canopy and topographic indicators (e.g., canopy height and density, elevation, slope, aspect, curvature, etc.) for the purpose of determining wood fiber attributes. Airborne LiDAR data were acquired over a one million hectare forest estate located in central Alberta, Canada, and a number of intrinsic indicators of wood properties were measured within field plots located throughout the area. We demonstrate how plot-level LiDAR canopy and terrain metrics can be used to predict plot-level averages of two synthetic wood fiber attributes obtained by a principal component analysis.

METHODS

Lodgepole pine (*Pinus contorta* var. *latifolia* Engelm.) is one of the most ubiquitous tree species in western North America, occurring in many different inland forest types of the montane and subalpine zones, often in spatially extensive pure stands, but also in mixed stands (Lotan and Critchfield, 1990). Ecologically, the successional role of lodgepole pine depends upon the local environmental conditions and extent of competition from associated species (Hardy et al. 1999). Since tree growth is strongly related to the availability of light, information on crown depth, tree spacing and stand density are potentially useful indicators for wood and fiber properties in lodgepole pine (Mansfield et al. 2007). Additionally, information on stand structure has also been related to stand and soil properties, and as a result, a better understanding of canopy architecture could be useful for determining the amount and value of merchantable timber and wood products (Mäkinen and Colin, 1998; Wilhelmsson et al. 2002).

The geographic area of focus of this study is a largely lodgepole pine dominated forest located in the Hinton Forest Management Area (FMA), which is managed by Hinton Forest Products, a division of West Fraser Timber, and located approximately 280 km west Edmonton, Alberta (53°25'N, 117°35'W). The mean annual temperature is about 4^{o}C, the mean annual precipitation is about 400 mm. The Hinton FMA contains a range of lodgepole pine age classes, management histories and disturbances; an overview is provided in Figure 1.

Insert Figure 1 about here:

Extrinsic and Intrinsic Descriptors of Wood Fiber Properties:

In 2001, 54 forest inventory plots (plot size 25 x 25m) were randomly sampled across the region to determine wood fiber properties as part of the Integrated Wood Properties Trend Assessment (IWQTA) program initiated by Weldwood of Canada's Hinton Division (Dempster and Burkell 2002). The stands were largely lodgepole pine dominated, however, some were mixed with black spruce (*Picea mariana* (Mill.) BSP) and white spruce (*Picea glauca* (Moench) Voss). The selection of the sites was based on their leading species, timber productivity rating and age class based on Weldwood's internal inventory record. At each plot, trees were selected using a prism (3, 4 or 5 prism basal area factor), such that 10 sample trees (living and > 7.0 cm DBH) for the target species were selected. A set of standard forest inventory variables were measured in each plot (all trees) (Dempster and Burkell 2002), including diameter at breast height (DBH), height, crown size and condition and branch dimensions of the largest branch up to 5 m from the ground (Table 1).

Insert Table 1 about here:

In addition to the standard inventory attributes, a number of wood fiber attributes were measured (Table 2). For all sample trees, two 12 mm diameter core (bark-to-bark) samples were extracted at breast height (1.3m) using a large diameter increment borer (Dempster and Burkell 2002). These core samples were labeled and placed in protective tubes for preparation and shipment to the laboratories for analysis. Cores were then pretreated with ethanol to remove water and other extractables (see Singleton et al. 2003 for detailed discussion on the effect of extraction on density estimates), and allowed to equilibrate to 20° C and 40% relative humidity prior to X-ray microdensitiometric analysis using the Silviscan®-2 (CSIRO, Australia) instrument. Age was estimated using dendrochronological methods providing an estimate of growth rate (defined as DBH / age). A brief description of the fiber attributes measured is provided in Table 2, with Zobel and Van Buijtenen (1989) and references therein providing additional information on their definition and other methods of measurement.

Insert Table 2 about here:

1. *Basic wood density (kg/m^3)* was calculated as the ratio of dry mass to green volume. Density is one of the most common indicators of solid-wood strength elasticity (Zobel and Van Buijtenen, 1989), rupture and pulp yield (Gartner, 2005; Lindström, 1996a, 1996b, 1996c; Downes and Drew, 2008). As density is integral to plant-level hydraulics and cavitation it has been shown to vary across species and geographically. It also varies within daily and seasonal time periods driven both by temperature and precipitation (Swenson and Enquist, 2007).

2. *Cell perimeter (µm)* (correlated with basic wood density) was calculated from the radial and tangential xylem cell diameters; it is known to have a strong influence on water transport and mechanical support (Dean and Long, 1986; Gartner, 2006; Baas et al. 2004). Wood fibers with larger

perimeters and thinner walls generally collapse more readily, and therefore make denser, stronger, and smoother paper (Wang and Aitken, 2001; Zobel and Van Buijtenen, 1989).

3. *Cell coarseness (µg/µm)* is the ratio of cell wall mass to cell unit length (µm) (Gartner, 2006) but can be approximated by fiber weight (µg) per unit length (m) (Via et al. 2004) by combining X-ray density profiles with cell diameter profiles. Research indicates that cell coarseness is strongly related to drought resilience (Hacke et al. 2001; Gartner, 2006), and influences paper strength and stiffness (Via et al. 2004), with improved paper qualities associated with low cell coarseness.

4. *Microfibril angle (°)* is the angle of the cellulose microfibrils with respect to the long axis of the individual cells (Wimmer et al. 2002). Microfibril angle (MFA) normally ranges from 5 - 20° in outer growth rings and varies depending on mechanical stress of the tree due to wind and gravity (Van Leeuwen et al. 2011). MFA is a key determinant of wood stiffness. Barnett and Bonham (2004), Wimmer et al. (2002) and Downes et al. (2002) found that MFA was larger in earlywood and juvenile wood and lower in latewood and mature wood

5. *Mature fiber length (µm)* is the length of the wood cell. This property influences paper and timber strength and stiffness. Longer fiber length, together with reduced cell coarseness, leads to improved bonding and is associated with paper strength and stiffness and pulp yield (Via et al. 2004). Fiber length is also an important attribute for timber products, since longer fibers result in greater resistance against buckling of wood beams; however, the trait is considered of lesser importance than wall thickness and wood density (Zobel and Van Buijtenen, 1989).

6. *Modulus of elasticity* is a measure of the resistance of wood to deformation under applied load and can be determined indirectly as a function of wood density Modulus of elasticity influences strength, and dimensional stability in structural lumber, and is used as an indicator of stiffness in machine stress grading of structural timber (Watt et al. 2006).

Fifty four plots were available from field inventory and used to determine the relationship between wood fiber characteristics and field attributes. The basal area-weighted average of values across the cores was used to describe the fiber attributes used in the following analyses. As indicated above, the sub-cellular structure of wood fiber attributes are often highly correlated. As a result, there is a degree of redundancy in the six attributes which can be reduced to produce overall assessment of the wood fiber properties. To address this redundancy, we applied a principal component analysis (PCA) to a variance/covariance matrix derived from the original six wood quality attributes to produce a subset of orthogonal (uncorrelated) attributes that describe most of the variance in the wood fiber dataset. To ensure each of the six wood fiber attributes were weighted equally, we first centered and scaled each attribute by its standard deviation (z-score). The PCA provides eigenvalues which can be used to order the principal components by the amount of variance explained in the observed fiber attributes. They can therefore be used to restrict the number of components to only those explaining significant (non-trivial) amounts of variation in the original dataset.

Airborne LiDAR acquisition and LiDAR Metrics:

Discrete return airborne LiDAR data were acquired on November 19th 2007, using an Optech 3100 sensor at a mean flying altitude of 1400 m. Only a subset of the area covering the entire 54 plots was flown, so that 21 of these plots were available from field measurements and LiDAR simultaneously. The sensor had a 70 kHZ pulse rate, recording up to 4 returns per outbound laser pulse. The estimated positional accuracy of the sensor was 0.45 and 0.30 m in horizontal and vertical direction, respectively.

The flying speed was 296 km/h; data were recorded with a scan frequency of 33 Hz and at an average point spacing of 0.75 m with a 50% overlap between flight lines. Ground and non-ground returns were separated using Terrascan v 0.6 (Terrasolid, Helsinki, Finland) (Kraus and Pfeifer, 1999) and a Digital Elevation Model was generated from the ground returns at a spatial resolution of 1 m (using a grid based software approach, Fusion v 2.65, USDA, Forest Service). To match the plot level information obtained from field measurements, and to allow processing of the LiDAR metrics from an operational standpoint, tree heights were first estimated using a 1m resolution DEM, and then averaged to the plot level by using 25 m spatial grid cells. Likewise, terrain heights were also averaged to match the wood fibre observations using a plot level size of 25 m.

Three sets of metrics were derived from the LiDAR point cloud: (1) topographic or terrain-related indices extracted from a gridded surface of bare-earth ground returns, (2) canopy height and density metrics, including Weibull location, scale, and shape parameters of the LiDAR canopy height distribution, and (3) bulk-canopy light metrics describing the depth and density of three hypothetical light zones.

(a) *Topographic indicators.* We created a 25 m digital elevation model (DEM) from all LiDAR points classified as ground returns, and then extracted estimates of elevation, slope, sine- and cosine corrected aspect (Stage and Salas, 2007). We selected these particular terrain metrics as potential indicators of resource availability and plant growth based on findings of previous studies (Franklin, 1995; Hengl and Reuter, 2009; Lookingbill and Urban, 2005; Wilson and Gallant, 2000).

(b) *Forest canopy height and density attributes* and *Weibull location, scale and, shape parameters* were computed at a 25 m grid-cell resolution using all LiDAR canopy height returns above 2m following the definitions and methods of Næsset (2004). Metrics included canopy cover (computed at 2m above the ground, at mean canopy height, and at modal canopy height), maximum canopy height, height percentiles from 10 to 90 %, and the first four *L*-moments of the canopy height distribution (i.e., mean, coefficients of variation, skewness, and kurtosis) (Frazer et al., 2011). All LiDAR canopy height and density metrics were computed using Fusion/LDV Version 2.8 developed by the United States Department of Agriculture, Forest Service, Pacific Northwest Research Station. The probability of canopy gap (gap fraction) at canopy height *z* was estimated as the sum of the total number of laser hits down to a height *z*, relative to the total number of within-plot LiDAR returns (N) (Coops et al. 2007; Lovell et al. 2003; Riano et al. 2003):

$$P_{gap}(z) = 1 - \frac{\sum_{z_j=z}^{z_j=z_{max}} \#z_j}{N} \quad (1)$$

where $\#z_j$ is the number of hits at height z_j, and j takes the value from height z to the top of the canopy at z_{max}.

Several different distributions can be fitted to the foliage density profile in order to characterize the vertical distribution of canopy elements. Most commonly a Weibull function is used, due to its flexibility in characterizing foliage distributions of various species (Kershaw and Maguire, 1995; Vose, 1988). This distribution has also been used (Magnussen et al. 1999) to examine the distribution of canopy heights from airborne LiDAR systems by comparing the probability of LiDAR height quantiles above a desired height with the distribution of leaf area. The Weibull cumulative density function can be related to the probability of a canopy gap as follows:

$$\frac{\delta P_{gap}(z)}{\delta z} = \theta \frac{z}{\kappa}^{\lambda-1} e^{\left(-\frac{z}{\theta}\right)^{\lambda}} \quad (2)$$

where κ, λ and θ are respectively shape, scale and location (height) parameters of the Weibull distribution. The height parameter may either be estimated or set to the height of the highest LiDAR return (Bailey and Dell, 1973). κ, λ and θ may be obtained from simple non-linear regression of the LiDAR returns per height layer (here, LiDAR data were grouped into 1m vertical strata), see Coops et al (2007) for details. Parameters of the Weibull distribution can then be empirically related to physical properties of interest (Coops et al. 2007; Lefsky et al. 1999; Parker et al. 2002).

(c) *Bulk-canopy light metrics.* We developed several new LiDAR metrics related to canopy light transmittance and interception, and the vertical partitioning of canopy light regimes based on the findings of three published studies: Magnussen and Boudewyn (1998), demonstrated that simple quantiles of laser canopy height were well correlated with the vertical distribution of stand leaf area. Lefsky et al. (1999) described a method of classification based on the presence/absence and vertical accumulation of laser return energy, that allowed partitioning of the canopy volume into regions of closed vs. empty (gap) space, and high (euphotic) vs. low (oligophotic) light. Finally, Parker et al. (2002) used the estimated means and variances of photosynthetically active radiation (PAR) measurements taken along a vertical axis from the top to the bottom of the canopy to separate the canopy profile into "bright" (high mean, low variance), "transition" (rapid change in mean PAR, high variance), and "dim" (low mean, low variance) light zones. By extension, we used a simple linear regression model of the form $\hat{Y} = b_0 + b_1X$ to fit a scatter plot of sample quantiles of LiDAR canopy height Lh_q (*Y*-axis) against q (*X*-axis) to approximate the boundary height (h_2) between 'bright' and 'transition' zones (i.e., $\hat{Y} = b_0 + b_1$) and the boundary height (h_1) between 'transition' and 'dim' zones (i.e., $\hat{Y} = b_0$) (Figure 5B). Prior to fitting the linear model, we arbitrarily trimmed the tails of the LiDAR canopy height distribution at the 10th (q = 0.1) and 90th (q = 0.9) percentiles in order the limit the influence of distributional outliers on model fit. In cases where b_0 was less than zero (i.e., $h_1 < 0$) and the sum of b_0 and b_1 was greater than the maximum LiDAR canopy height (i.e., $h_2 > Lh_{100}$), we set $h_1 = 0$ and $h_2 = Lh_{100}$. From estimates of h_1 and h_2, we computed five separate metrics: (1) thickness (m) of the 'bright' zone ($Lh_{100} - h_2$); (2) thickness (m) of the 'transition' zone ($h_2 - h_1$); (3) thickness (m) of the 'dim' zone (h_1); (4) canopy density (%) above h_1; (5) canopy density (%) above h_2. We expected that metrics (2) and (4) are important predictors of wood properties because the 'transition' zone contains the bulk of canopy leaf area, and is therefore an important functional zone influencing several key canopy processes related to plant growth (e.g., light capture, photosynthesis, evapotranspiration, material exchanges) (Parker et al., 2002).

Statistical Approach:

We used stepwise multiple linear regression to systematically add or remove terms from the multi-linear regression between LiDAR metrics and the non-trivial principal components (PC's) derived from the wood fiber dataset (response) based on their statistical significance. The approach compares the explanatory power of an initial regression model to incrementally larger and smaller models based on the p value of an F-statistic. The method terminates when no single step improves the model (Draper and Smith, 1998). LiDAR attributes were extracted for all plot locations at which field measurements of wood fiber attributes had been acquired included measures of the terrain structure (elevation, slope and aspect), measures of the radiation regime (thickness of bright, transition and dim canopy zones), and the canopy structure itself (tree height and foliage distribution as indicated by the Weibull parameters). Based on the results of previous studies (Franklin, 1995; Hengl and Reuter, 2009; Lookingbill and Urban, 2005; Wilson and Gallant, 2000) and a review by van Leeuwen et al. (2011), these metrics were then used as indicators of fiber strength, smoothness and softness and related to the principal components derived from tree core observations.

RESULTS

Results from a PCA of the intrinsic indicators of wood fiber attributes indicated that only two PCs were statistically significant (Figure 2). Wood strength and stiffness (PC1) was related to the depth of canopy measured by length and beginning of the green tree crown and the canopy profile description. Fiber yield (PC2) was related to tree height and tree height distribution as provided by the LiDAR canopy metrics. The first PC accounted for 53.2% of the total variance in the 6 attributes, while PC2 accounted for 34.4% of the total variance. As a result, the first two PCs combined explained over 87.6% of the total variance in the wood fiber dataset.

Insert Figure 2 about here:

PC1 predominantly captures variations in wood density and modulus of elasticity (MOE). A low MOE indicates that low force is required to achieve deflection, which can be interpreted as high elasticity or low stiffness. Consequently, this first PC can be described as an indicator of wood strength, stiffness and fiber quantity (Gartner, 2005). PC2 describes differences in fiber dimension (i.e. cell perimeter, coarseness, and length), with increases in PC2 associated with increases in cell coarseness, perimeter, and length. PC2 may therefore be interpreted as an indicator of the overall fiber strength, smoothness and softness (Gartner, 2005). Figure 3 shows the eigenvalues all six principal components, Table 3 shows the component loadings, correlations for those non-trivial principal components (PC1 and PC2)

Insert Figure 3 about here:
Insert Table 3 about here:

The relationships between selected field-based inventory measurements and the first two PCs derived from the wood fiber attributes are shown in Figure 4. Based on our regression analysis, the first PC, describing wood strength, stiffness, and fiber yield, was significantly correlated (R^2 = 0.65) with the annual increment in DBH, and PC2, an indicator of fiber strength, smoothness, and softness of the wood fiber, was significantly correlated (R^2 = 0.73) with stand height.

Insert Figure 4 about here

Figure 5a provides an example of a LiDAR-derived foliage density profile estimated for a single plot. The histogram of observed LiDAR canopy returns is shown as gray bars, and plotted in steps of one meter canopy height increments, with the fitted Weibull function shown in black. For the example shown in Figure 5a, the majority of foliage is located between 12 and 18 meters in height, with only little understory present in this stand. The fitted Weibull curve captured the distribution of the foliage well, while smoothing the observed distribution of foliage towards the upper end of the canopy. Figure 5b shows the quantiles of a cumulative foliage density profile, and linear regression model fit to the 10^{th} to 90^{th} percentiles of LiDAR canopy height. The slope and *y*-intercepts of the regression line approximate the bright, transition, and dim canopy zones described by Parker et al. (2002). While this technique does not provide an absolute estimate of canopy density at a given height level (compare Figure 5a) the method was able to describe the relative distribution of foliage within the canopy.

Maps of canopy properties are provided in Figure 6. Figure 6a provides maps of the Weibull coefficients (shape parameter, scale parameter and location parameter) across the entire LiDAR dataset whereas Figure 6b shows the corresponding canopy zones (bright, transition and dim) for the same region. The

observed Weibull fittings were dominated by the scale parameter (λ) in most regions, whereas the mountainous regions were dominated by a combined effect of λ and κ (Figure 6a). Additionally, the dim canopy zone was more predominant in lower regions but not in higher mountain areas (Figure 6b).

Insert Figure 5 about here:
Insert Figure 6 about here:

Canopy heights (95th percentile of all LiDAR returns) and terrain properties observed by the LiDAR data at the site are presented in Figure 7. Stand heights varied between 0 and 39.8 m, terrain elevation varied between 783 and 2386 m. Of the LiDAR derived terrain, canopy and light metrics, only the light metrics, that is the thickness of the upper canopy zone (bright), relative to the total canopy height was significantly correlated to PC1 (r^2 = 0.55, $p < 0.05$). The stepwise multiple regression indicated an F value of 20.3654, ($p<0.01$) for lidar derived metric of the upper canopy, whereas other measures of terrain and canopy structure did not significantly improve the regression ($p> 0.3$ for all other terrain and canopy metrics). The root mean square error for the regression to PC1 was 0.9526. PC2 was significantly correlated to the height (95th percentile of all LiDAR returns) of the canopy and the total thickness of the canopy (RMSE = 0.8393 and RMSE= 0.7509, respectively). (r^2 = 0.65, $p < 0.05$). The F statistics for the regression indicated a value of 20.3102, the p values where $p<0.001$ and $p< 0.027$, respectively. Again, none of the terrain metrics improved the prediction model significantly and were therefore excluded from the stepwise regression. Figure 8 shows the relationship between LiDAR observed stand attributes and the two principal components derived from the wood fiber attributes.

Insert Figure 7 about here:
Insert Figure 8 about here:

Figure 9 shows the LiDAR derived model of the first two principal components of the wood fiber attributes across the entire study area (using the model presented in Figure 8). Harvested areas are excluded from this graph (shown in white).
By assigning the key predicted fiber components to different colors the combined image provides information on the overall patterns of wood fiber properties over the study area. Fiber strength, smoothness, and softness, shown in red, stiffness, and fiber yield is displayed as variations of green.

Insert Figure 9 about here:

DISCUSSION

Previous research has demonstrated the statistical relationships between individual-tree measurements (i.e., DBH, tree height, growth, and crown dimensions), stand structure, site characteristics (climate, topography, nutrient availability), and wood fiber properties, (van Leeuwen et al. 2011 and references therein) as well as between wood fiber attributes and site and stand level variables (e.g., stocking density) or broader climate and soil environmental characteristics. These relationships also appear evident in this dataset, with stand height and growth variables all found to be significantly related to synthetic wood fiber attributes across the sampled plots. While the core samples were selected from trees that were representative of the study area, factor loadings derived from the principal components are specific to the area they are representative of and can therefore not easily be transferred to other forest types. Other vegetation systems may therefore yield different loadings or different prediction parameters.

Conventionally, airborne LiDAR data has been used successfully to predict a range of forest crown and canopy structural attributes, including crown width, length, and height-to-first-living branch (Hopkinson

et al. 2006; Chasmer et al. 2006; Riano et al. 2004; Morsdorf et al. 2004; Andersen et al. 2005; Solberg et al. 2006), as well as biomass increment (Bollandsas and Næsset, 2009). The link to wood fiber attributes has not yet been fully explored; however, Suarez et al. (2010), for example, demonstrated the use of the Canadian TASS model in combination with the Timber Quality for Conifers (ConTQ) model to derive estimates of timber properties from LiDAR data. In addition, a variety of recent studies have focused on quantifying branch structure and pattern and crown depth from LiDAR data, with the direct aim of improving wood fiber attribute estimation. The prediction rates for the two principal components were 55% and 69%, respectively. While this result is statistically significant ($p<0.05$), a notable variability in both PCs has not be explained by LiDAR derived variables, suggesting that prediction capacities of airborne LiDAR are somewhat limited. However, the support of terrestrial LiDAR could potentially help to improve these results further (Hilker et al., 2011). It is noteworthy that most of the predictive power stemmed from LiDAR derived metrics of the light regime. This results not only demonstrates the potential of the new, radiation based metrics introduced in this study to predict growth rates (dbh increment), but also underlines the importance of the crown size and structure for high fiber quality. Similar, continental climate throughout the study area is the most likely cause for the low explanatory power of the terrain derived metrics, with strong seasonal effects driving plant growth rather than terrain aspect. Five to ten percent in predictive capacity was lost when using LiDAR data compared to field observations. One potential reason is that LiDAR based predictions were validated only for a subset of plots, since the availability of coinciding LiDAR and field measurements was limited to 21 stands. While this is a certain limitation of the given dataset, all measurements were sampled within the same ecotone, elevation range and using the same species distribution in the Albertan foodhills. Most likely, however, the loss in predictive capacity is due to the fact that while height related metrics can be accurately observed from LiDAR directly, estimation of stem volume related measures components, such as DBH are more difficult to quantify. Terrestrial laser scanning may help to improve remotely sensed predictions of fiber quality as the “bottom up” approach of terrestrial systems allows a more detailed assessment of the below canopy architecture, including the magnitude of the shaded tree canopy.

As shown in this study, bulk-canopy light metrics, that provide an indication of the canopy light regimes, were significant predictors of site-level differences in wood density, modulus of elasticity, and microfibril angle. In addition to previously published canopy metrics (Coops et al., 2007), the newly introduced light metrics yielded a significantly enhanced prediction of canopy structure and wood fiber attributes. These three wood fiber components are considered to be key indicators of wood stiffness, strength, and fiber quantity. LiDAR canopy height and density metrics were important in quantifying differences in fiber dimension (i.e., cell perimeter coarseness, and mature fiber length). Of particular interest is the relationship between the plot- level inventory attributes, bulk-canopy light metrics, and the first principal component focused on wood strength, stiffness, and fiber yield. Simple correlation analysis identified DBH increment as the most significant variable in describing variance in this wood fiber principal component. As no increment data is readily extractable from a single pass LiDAR dataset, information on the crown light regimes, modeled as the depth of the transition, bright and dim zones provided a good predictive model. Future research may include other, perhaps more sophisticated radiation models would allow to explore the impact of radiation on wood fiber quality more in detail.

It is acknowledged that this dataset also presented some additional challenges in the mapping of wood fiber characteristics and properties. Field measurements and wood fiber attributes were collected in 2001 whereas the LiDAR acquisition did not occur to 2007 resulting in a six year time difference between datasets. It is recognized that this is likely to have diminished the predictive capability of the models developed. In addition to this, the process of extracting wood fiber attributes through destructive sampling techniques could cause structural variations and disturbance within the stand, which may

affect how successfully these models can be transferred to other stands. On the other hand, the low productivity of the sites also limits the impact of the time difference between field and LiDAR observations. So far, this study has only investigated the effects of stand structural information on wood fiber attributes in mature lodgepole pine. The models established in this paper could vary with species, age class and stand composition. Further study is required to address these current limitations.

Airborne LiDAR is becoming increasingly available and is now being acquired routinely in several countries for inventory purposes (e.g. Næsset et al., 2004). The results of this study suggests that LiDAR data could be useful for predicting wood fiber attributes from airborne observations which would allow an enhanced planning and marketing of timber products pre-harvesting.

CONCLUSION

This study has shown that airborne LiDAR provides opportunities for the broad scale characterization of wood quantity and quality. One of the most important quantities observed from LiDAR is the vertical distribution of foliage within the canopy, referred to in this manuscript as the foliage density profile. Our results show that airborne LiDAR variables can explain approximately half of the observed variance in wood fiber attributes, which is approximately 5 – 10 % less than that explained by ground-based inventory variables, such as diameter increment and height. This small reduction in explained variance should be considered in the context of the significant opportunities LiDAR provides for broader spatial characterizations of wood quantity and quality at the stand and landscape level.

REFERENCES

Andersen, H.-E., McGaughey, R.J., Reutebuch, S.E., 2005. Estimating forest canopy fuel parameters using LIDAR data. *Rem. Sens. Env*. 94, 441-449.

Baas, P., Blokhina, N., Fujii, T., Gasson, P., Grosser, D., Heinz, I., Ilic, J., Xiaomei, J., Miller, R., Newsom, L.A., Noshiro, S., Richter, H.G., Suzuki, M., Terrazas, T., Wheeler, E., & Wiedenhoeft, A. (2004). IAWA list of microscopic features for softwood identification. *IAWA Journal, 25*, 1-70

Bailey, R.L., Dell, T.R., 1973. Quantifying diameter distributions with weibull function. Forest Science 19, 97-104Barnett, J.R., Bonham, V.A., 2004. Cellulose microfibril angle in the cell wall of wood fibers. *Biological Reviews* 79, 461-472

Blair, J., Coyle, D., Bufton, J., & Harding, D. (1994). Optimization of an airborne laser altimeter for remote sensing of vegetation and tree canopies. In (pp. 939-941)

Bollandsas, O.M., Næsset, E., 2009. Weibull models for single-tree increment of Norway spruce, Scots pine, birch and other broadleaves in Norway. *Scandinavian Journal of Forest Research* 24, 54-66

Bucksch, A., Fleck, S., 2009. Automated detection of branch dimensions in woody skeletons of leafless fruit tree canopies. *SilviLaser 2009*, Oct 14 – 16, Austin, Texas.

Bucksch A & R Lindenbergh (2008) CAMPINO - A skeletonization method for point cloud processing. *ISPRS J Photogramm Remote Sens*, 63, pp. 115-127

Chasmer, L., Hopkinson, C., Treitz, P., 2006. Investigating Laser Pulse Penetration Through a Conifer Canopy by Integrating Airborne and Terrestrial Lidar. Can. J. Rem. Sens. 32, 116-125.

Chen, F., Evans, R., 2005. A robust approach for vessel identification and quantification in eucalypt pulpwoods. *Appita J.* 58, 442-447.

Chen, F., Evans, R., 2010. Automated measurement of vessel properties in birch and poplar wood. *Holzforschung*, 64, 369-374.

Chhin, S., Hogg, E.H., Lieffers, V.J., Huang, S., 2008. Influences of climate on the radial growth of lodgepole pine in Alberta. *Botany* 86: 167-178.

Coops, N. C., Hilker, T., Wulder, M. A., St-Onge, B., Newnham, G., Siggins, A., Trofymow, J. A., 2007. Estimating Canopy Structure of Douglas-fir Forest Stands from Discrete-Return LiDAR. *Trees* 21,

295-310.
Danson, F.M., Hetherington, D., Morsdorf, F., Koetz, B., Allgöwer, B., 2007. Forest canopy gap fraction from terrestrial laser scanning. *IEEE Geosci. Rem. Sens. Lett*. 4, 157-160.
Dean, T.J., Long, J.N., 1986. Validity of Constant-stress and Elastic-instability Principles of Stem Formation in Pinus contorta and Trifolium pretense. *Ann. Bot*. 58, 833-840.
Dempster, W.R., Burkell, G. 2002. Weldwood Alberta Fiber Quality Forecasting FRIAA Project 95 WELD-01-88 *Technical Report*. 27 pp.
Donaldson, L., 2008. Microfibril Angle: Measurement, Variation And Relationships - A review. *IAWA J.* 29, 345-386.
Downes, G.M., Drew, D.M., 2008. Climate and growth influences on wood formation and utilization. *South. For*. 70, 155-167.
Downes, G.M., Wimmer, R., Evans, R., 2002. Understanding wood formation: gains to commercial forestry through tree-ring research. *Dendrochronologia* 20, 37-51.
Draper, N. R., Smith, H., 1998. *Applied Regression Analysis*. Hoboken, NJ: Wiley-Interscience, 1998. pp. 307–312.
Eriksson, D., Lindberg, H., Bergsten, U., 2006. Influence of silvicultural regime on wood structure characteristics and mechanical properties of clear wood in Pinus sylvestris. *Silva Fennica*, 40, 743-762.
Evans, R., Ilic, J., 2001. Rapid prediction of wood stiffness from microfibril angle and density. *For. Prod. J.* 51, 53-57.
Evans, R., Stringer, S., Kibblewhite, R.P., 2000. Variation of microfibril angle, density and fiber orientation in twenty-nine Eucalyptus nitens trees. *Appita J.* 53, 450–457.
Franklin, J., 1995. Predictive vegetation mapping: geographic modelling of biospatial patterns in relation to environmental gradients. *Progress in Physical Geography* 19: 474-499.
Frazer, G. W., Magnussen, S., Wulder, M. A., & Niemann, K. O. (2010). Simulated impact of sample plot size and co-registration error on the accuracy and uncertainty of LiDAR-derived estimates of forest stand biomass. *Remote Sensing of Environment, 115*(2), 639-649.
Gartner, B.L., 2005. Assessing wood characteristics and wood quality in intensively managed plantations. *Journal of Forestry* 103(2): 75–77.
Gartner, B.L., 2006. Predictions of Wood Structural Patterns in Trees by Using Ecological Models of Plant Water Relations, in: Characterization of the Cellulosic Cell Wall, Stokke, D.D., Groom, L. H. (Eds), Blackwell Publishing, Ames, Iowa, pp. 274.
Hacke, U.G., Sperry, J.S., Pockman, W.T., Davis, S.D., McCulloh, K.A., 2001. Trends in Wood Density and Structure Are Linked to Prevention of Xylem Implosion by Negative Pressure. *Oecologia* 126, 457-461.
Hardy, C.C., Keane, R.E., Stewart, C.A., 1999. Ecosystem-based management in the lodgepole pine zone. Bitterroot Ecosystem Management Research Project: What We Have Learned, 31-35.
Hengl, T., and Reuter, H.I., 2009. Geomorphometry: Concepts, Software, Applications. Elsevier, Amsterdam. 765 pp.
Hilker, T., van Leuuwen, M., Coops, N.C., Wulder, M.A., Newnham, G.J., Jupp, D.L., Culvenor, D.S., 2010. Comparing canopy metrics derived from terrestrial and airborne laser scanning in a Douglas-fir dominated forest stand. *Trees* 24, 819–832
Hilker, T., Coops, N.C., Newnham, G.J., van Leuuwen, M., Wulder, M.A., Steward, J., Culvenor, D.S. (2011). Comparison of terrestrial and airborne LiDAR in describing stand structure of a thinned lodgepole pine forest. *Journal of Forestry, in press*
Holmgren J & Å Persson (2004) Identifying species of individual trees using airborne laser scanner. *Remote Sensing of Environment, 90*, pp. 415-42
Hopkinson C., Chasmer, L., Young-Pow, C., Treitz, P., 2004. Assessing forest metrics with a ground-based

scanning LiDAR. *Can. J. Rem. Sens*. 34, 573-583.
Hopkinson, C., Chasner, L., Lim, K., Trietz, P., Creed, I., 2006. Towards a universal lidar canopy height indicator. *Can. J. Rem. Sens*. 32, 139-152.
Huang, P., Pretzsch, H., 2010. Using terrestrial laser scanner for estimating leaf areas of individual trees in a conifer forest. *Trees-Structure and Function* 24, 609-619
Jupp, D.L.B., Culvenor, D.S., Lovell, J.L., Newnham, G.J., Strahler, A.H., & Woodcock, C.E., 2009. Estimating forest LAI profiles and structural parameters using a ground-based laser called 'Echidna'. *Tree Phys*. 29, 171-181.
Kershaw, J.A., Maguire, D.A., 1995. Crown structure in western hemlock, Douglas-fir, and grand fir in western Washington: Trends in branch-level mass and leaf area. *Can. J. For. Res*. 25, 1897-1912.
Kint, V., Hein, S., Campioli, M., Muys, B., 2010. Modelling self-pruning and branch attributes for young *Quercus robur* L. and *Fagus sylvatica* L. trees. *Forest Ecol. Manage*. 260, 2023–2034.
Kraus, K., Pfeifer, N., 1999. Determination of terrain models in wooded areas with airborne scanner data. *ISPRS J. Photogramm. Remote Sens*. 54, 193-203.
Lefsky, M.A., Cohen, W.B., Acker, S.A., Parker, G.G., Spies, T.A., Harding, D., 1999. Lidar Remote Sensing of the Canopy Structure and Biophysical Properties of Douglas-Fir Western Hemlock Forests. *Rem. Sens. Env*. 70, 339-361.
Lefsky, M.A., Hudak, A.T., Cohen, W.B., Acker, S.A., 2005. Geographic Variability in Lidar Predictions of Forest Stand Structure in the Pacific Northwest. *Remote Sensing of Environment* 95, 532-548
Lim, K., Treitz, P., Wulder, M., St-Onge, B., Flood, M., 2003. LiDAR remote sensing of forest structure. *Prog. Phys. Geogr.* 27, 88-106.
Lindström, H., 1996a. Basic density in Norway spruce. Part I. A literature review. *Wood and Fiber Sci*. 28, 15-27.
Lindström, H., 1996b. Basic density of Norway spruce. Part II. predicted by stem taper, mean growth ring width, and factors related to crown development. *Wood and Fiber Sci*. 28, 240-251.
Lindström, H., 1996c. Basic density in Norway spruce. Part III. Development from pith outwards. *Wood and Fiber Sci.* 28, 391-405.
Lookingbill, T. & D. Urban. 2005. Gradient analysis, the next generation: Towards more plant-relevant explanatory variables. *Canadian Journal of Forest Research* 35:1744-1753.
Lotan, J.E. and W.B. Critchfield. 1990. Pinus contorta (Dougl. ex. Loud.). In R.M. Burns and B.H. Honkala (eds.). Silvics of North America. Vol. 1. Conifers, Agric. Handb. 654. pp. 302-315. USDA For. Serv., Washington, DC.
Lovell, J.L., Jupp, D.L.B., Culvenor, D.S., Coops, N.C., 2003. Using Airborne and Ground-Based Ranging Lidar to Measure Canopy Structure in Australian Forests. *Can. J. Rem. Sens*. 29, 607-622
Maas H.-G., Bienert, A., Scheller, S., Keane, E., 2008. Automatic forest inventory parameter determination from terrestrial laser scanner data. *Int. J. Rem. Sens*. 29, 1579-1593.
Magnussen, S., Boudewyn, P., 1998. Derivations of stand heights from airborne laser scanner data with canopy-based quantile estimators. Can. J. For. Res. 28, 1016-1031.
Magnussen, S., Eggermont, P., & LaRiccia, V. (1999). Recovering tree heights from airborne laser scanner data. *Forest Science, 45*, 407-422
Mäkinen, H., Colin, F., 1998. Predicting branch angle and branch diameter of Scots pine from usual tree measurements and stand structural information. *Can. J. For. Res*. 28, 1686-1696.
Mansfield, S.D., Parish, R., Goudie, J.W., Kang, K. Ott, P., 2007. The effects of crown ratio on the transition from juvenile to mature wood production in lodgepole pine in western Canada. *Can. J. For. Res.* 37, 1450-1459.
Morsdorf, F., Meier, E., Koetz, B., Klaus, I., Dobbertin, M., Allgoewer, B., 2004. LIDAR-based geometric reconstruction of boreal type forest stands at single tree level for forest and wildland fire management. *Rem. Sens. Env*. 92, 353-362.

591 Murphy, G., 2008. Determining stand value and log product yields using terrestrial lidar and optimal
592 bucking: A case study. *J. For*. 106, 317-324.
593 Næsset, E., 1997. Determination of Mean Tree Height of Forest Stands Using Airborne Laser Scanner
594 Data. *ISPRS J. Photogramm. Remote Sens*. 52, 49-56.
595 Næsset, E., 2002. Predicting forest stand characteristics with airborne scanning laser using a practical
596 two-stage procedure and field data. *Rem. Sens. Env.* 90, 88-99.
597 Næsset, E., Økland, T., 2002. Estimating tree height and tree crown properties using airborne scanning
598 Næsset, E.; Gobakken, T.; Holmgren, J.; Hyyppa, H.; Hyyppa, J.; Maltamo, M.; Nilsson, M.; Olsson, H.;
599 Persson, A., and Soderman, U. Laser Scanning of Forest Resources: The Nordic Experience.
600 *Scandinavian Journal of Forest Research*. 2004; 19:482-499.
601 Parker, G.G., Davis, M.M., Chapotin, S.M., 2002. Canopy light transmittance in Douglas-fir–western
602 hemlock stands. *Tree Physiology* 22, 147-157.
603 Parker, D.C., Manson, S.M., Janssen, M.A., Hoffman, M.J., Deadman, P., 2002. Multi-agent systems for
604 the simulation of land-use and land-cover change: A review. *Annals Of The Association Of*
605 *American Geographers.* 93: 2. Pages: 314-337
606 Persson, A., Holmgren, J., Söderman, U., 2002. Detecting and Measuring Individual Trees Using an
607 Airborne Laser Scanner. *Photogramm. Eng. Rem. Sens*. 68, 925-932.
608 Presslee, D.J., Navratil, S., 1998. Stand density management of lodgepole pine: a dilemma and options.
609 Stand Density Management: Planning and Implementation Proceedings, 124-130.
610 Riano, D., Chuvieco, E., Condes, S., Gonzalez-Matesanz, J., Ustin, S.L., 2004. Generation of crown bulk
611 density for Pinus sylvestris L. from lidar. *Rem. Sens. Env*. 92, 345-352.
612 Riano, D., Meier, E., Allgower, B., Chuvieco, E., Ustin, S.L., 2003. Modeling Airborne Laser Scanning Data
613 for the Spatial Generation of Critical Forest Parameters in Fire Behavior Modeling. *Remote Sens.*
614 *Environ.* 86, 177-186.
615 Schoennagel, T., Turner, M.G., Romme, W.H., 2003. The influence of fire interval and serotiny on
616 postfire lodgepole pine density in Yellowstone National Park. *Ecology*, 84, 2967-2978.
617 Schoennagel, T., Veblen, T., Romme, W., 2004. The interaction of fire, fuels, and climate across Rocky
618 Mountain forests. *BioScience*, 54, 661-676.
619 Singleton, R., DeBell, D.S., Gartner, B.L., 2003. Effect of extraction on wood density of western hemlock
620 (*Tsuga heterophylla* (Raf.) Sarg.). Wood and Fiber Science 35(3): 363–369.
621 Solberg, S., Næsset, E., Bollandsas, O.M., 2006. Single Tree Segmentation Using Airborne Laser Scanner
622 Data in a Structurally Heterogeneous Spruce Forest. *Photogramm. Eng. Rem. Sens*. 72, 1369-
623 1378.
624 Spies, T.A., Franklin, J.F., Thomas, T.B., 1988. Coarse woody debris inn Douglas-fir forests of western
625 Oregon and Washington. *Ecology* 69, 1689-1702.
626 Suarez, J.C., Gardiner, B.A., Di Luca, M., Goudie, J., Polsson, K., 2010. Consequences of stand structure
627 on timber quality. In: Silvilaser 2010, September 14–17, Freiburg, Germany.
628 Swenson, N.G., Enquist, B.J., 2007. Ecological and evolutionary determinants of a key plant functional
629 trait: wood density and its community-wide variation across latitude and elevation. *Am. J. Bot.*
630 94, 451-459.
631 Tansey, K., Selmes, N., Anstee, A., Tate, N.J., Denniss, A., 2009. Estimating tree and stand variables in a
632 Corsican Pine woodland from terrestrial laser scanner data. *Int J Remote Sens* 30, 5195–5209.
633 Thies, M., Pfeifer, N., Winterhalder, D., Gorte, B.G.H., 2004. Three-dimensional reconstruction of stems
634 for assessment of taper, sweep, and lean based on laser scanning of standing trees.
635 *Scandinavian J For Res* 19, 571-581.
636 Väisänen, H., Kellomäki, S., Oker-Blom, P., Valtonen, E., 1989. Structural development of Pinus sylvestrís
637 stands with varying initial density: A preliminary model for quality of sawn timber as affected by
638 silvicultural measures. *Scand. J. For. Res*. 4, 233-238.

639 Van Leeuwen, M., Hilker, T., Coops, N.C., Frazer, G., Wulder, M.A., Newnham, G.J., Culvenor, D.S., 2011.
640 Assessment of standing wood and fiber quality using ground and airborne laser scanning: A
641 review. *Forest Ecol. Manag*. 261. 1467-1478.
642 Via BK, M Stine, TF Shupe, S Chi-Leung & L Groom (2004) Genetic Improvement of fiber length and
643 coarseness based on paper product performance and material variability – a review. *IAWA*
644 *Journal,* 25, pp. 401.
645 Vose, J.M., 1988. Patterns of leaf-area distribution within crowns of nitrogen-fertilized and phosphorus-
646 fertilized loblolly-pine trees. Forest Sci. 34, 564-573.
647 Wang, T., Aitken, S.N., 2001. Variation in xylem anatomy of selected populations of lodgepole pine. Can.
648 *J. For. Res*. 31, 2049-2057.
649 Waring, R.H., Schroeder, P.E., Oren, R., 1982. Application of the pipe model theory to predict canopy leaf
650 area. *Can. J. For. Res*. 12, 556–560
651 Watt, M.S., Moore, J.R., Façon, J., Downes, G.M., Clinton, P.M., Coker, G., Davis, M.R., Simcock, R.,
652 Parfitt, R.L., Dando, J., Mason, E.G., Bown, H.E., 2006. Modelling the influence of stand
653 structural. edaphic and climatic influences on juvenile Pinus radiata dynamic modulus of
654 elasticity. *For. Ecol. Manag*. 229, 136-144.
655 Wei, X., Liu, W., Waterhouse, J., Armleder, M., 2000. Simulations on impacts of different management
656 strategies on long-term site productivity in lodgepole pine forests of the central interior of
657 British Columbia. *Forest Ecol. Manag*. 133, 217-229.
658 Wilhelmsson, L., Arlinger, J., Spangberg, K., Lundqvist, S.-O., Grahn, T., Hedenberg, O., Olsson, L., 2002.
659 Models for Predicting Wood Properties in Stems of Picea abies and Pinus sylvestris in Sweden.
660 *Scand. J. For. Res*. 17, 330-350.
661 Wilson, J.P., Gallant, J.C., 2000. Terrain Analysis: Principles and Applications. Wiley, New York, NY. 303
662 pp.
663 Wimmer R. 2002. Wood anatomical features in tree-rings as indicators of environmental change.
664 *Dendrochronologia,* 20, pp. 21.
665 Zobel, B.J., Van Buijtenen, J.P., 1989. Wood variation - its causes and control. Springer Verlag: Berlin, pp
666 363.
667

668

669 **TABLES:**

670 Table 1: Summary of forest field inventory data. The arithmetic mean and range of observations is
671 shown. The branch diameter is defined as the diameter of largest branch within 5 m of the ground (N =
672 54)

	stems/ha	%live crown	DBH (cm)	Height (m)	Age (years)	DBH increment (cm/year)	site index	branch diameter (cm)	crown diameter (m)
mean	1863.97	42.93	22.11	18.17	89	2.45	14	2.6	1.12
min	728	21.66	12.01	12.71	38	0.72	8	0.6	0.52
max	4486	63.85	34.76	26.47	224	5.85	20	4.2	1.96

673

674

675 Table 2: Summary of wood fiber attributes. The arithmetic mean and range of observations is shown.
676 DEN is the conditioned wood density (kg/m^3); PER is the cell perimeter (µm); CRS describes the cell
677 coarseness (µg/m); MFA is the microfibril angle (°); MOE describes the modulus of elasticity (GPa), and
678 MFL is the mature fiber length (mm). N = 54.

	DEN	PER	CRS	MFA	MOE	MFL
mean	496.2	107.5	340.8	15.5	13.3	2.4
min	454.7	100.5	310.4	12.1	108	2.2
max	548.8	114.4	392.2	19.1	15.6	2.6

679

680 Table 3: Component loadings for non-trivial principal components (N = 21). Abbreviations as in Table 2.

681

	PC1	PC2
DEN	-0.52	-0.05
PER	0.38	0.48
CRS	-0.20	0.57
MFA	0.44	-0.33
MFL	0.25	0.54
MOE	-0.53	0.18

682

683

684

685

686

687 **Figures**

688

689

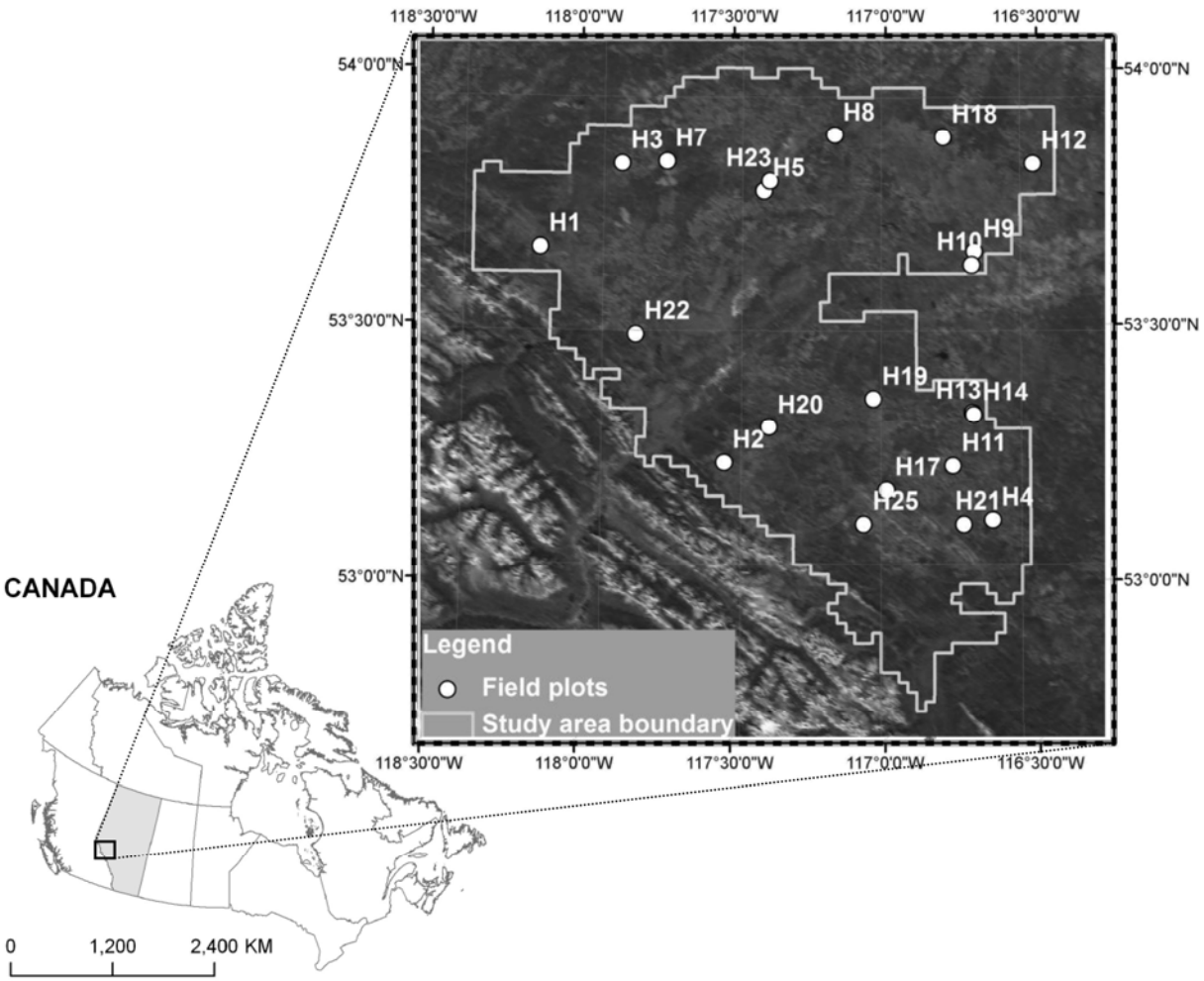

690

691

692 Figure 1: Map of Study Area overlaid on a MODerate Imaging Spectoradiometer (MODIS) satellite image

693

694

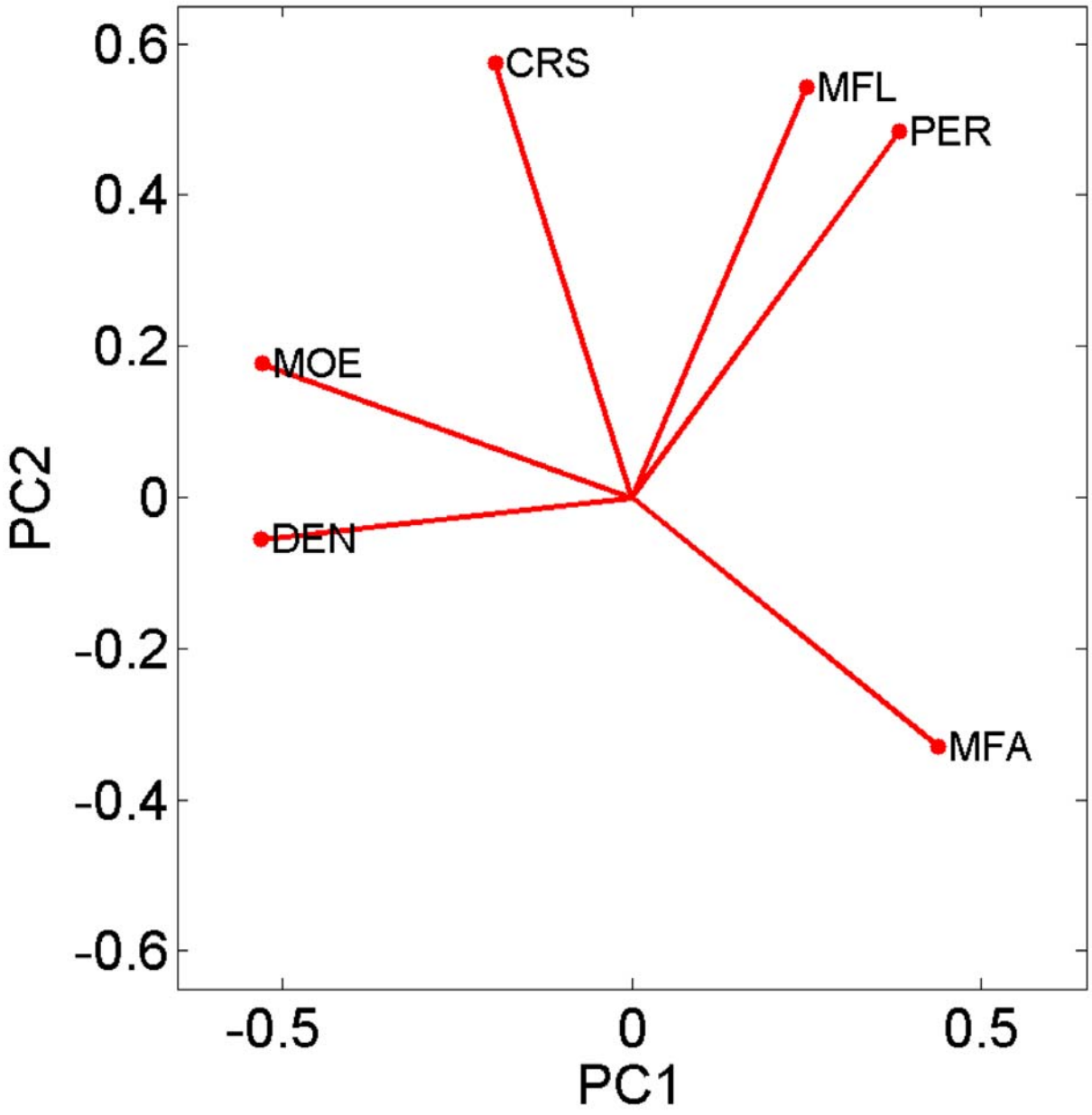

695

696

697 Figure 2: Magnitude and direction of the relationship between the field measured wood fiber attributes

698 and the principal components 1 and 2 (PC coefficients).

699

700

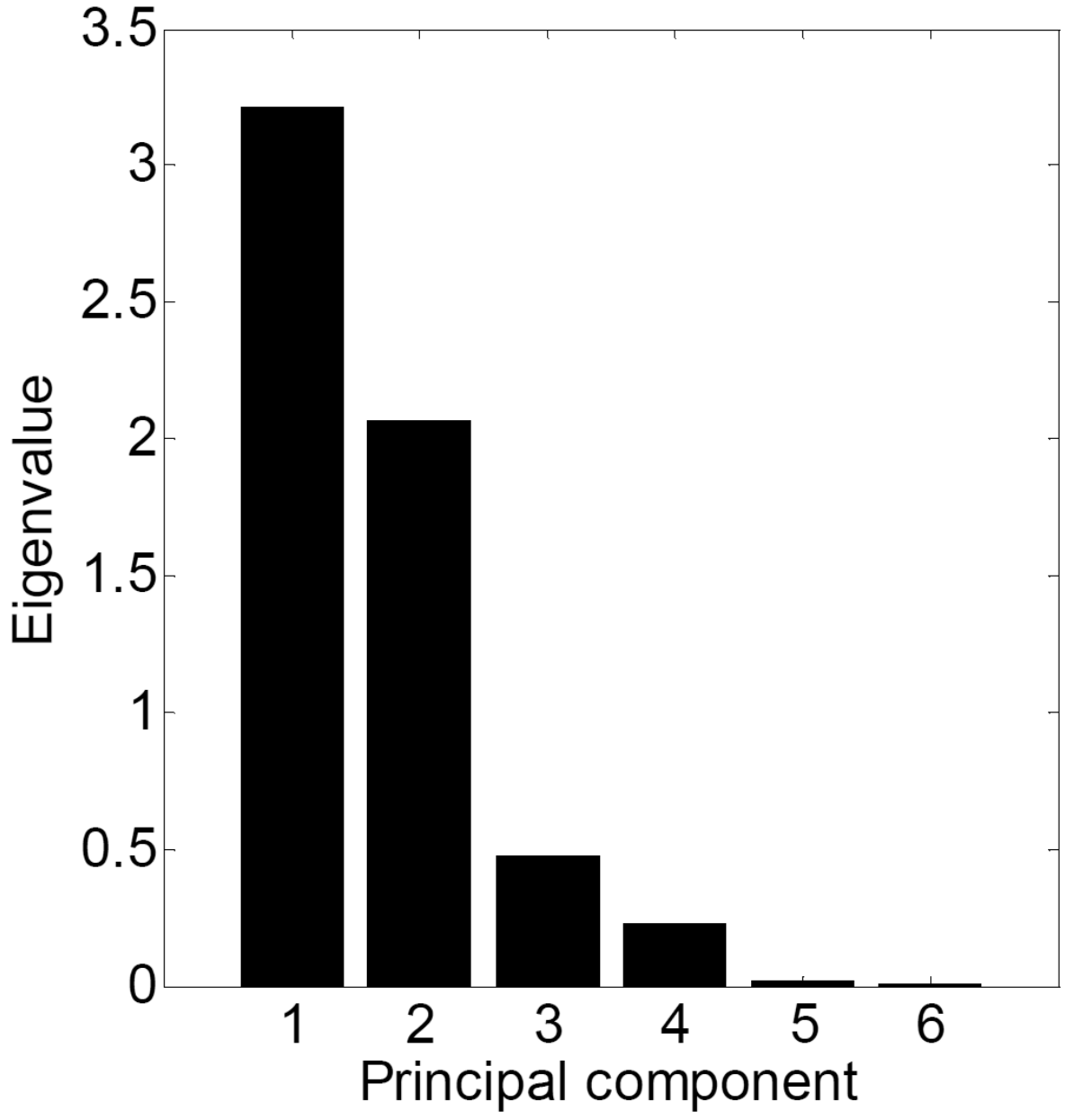

701

702

703 Figure 3: Eigenvalues for the principal component analysis performed on the field observations

704

705

706

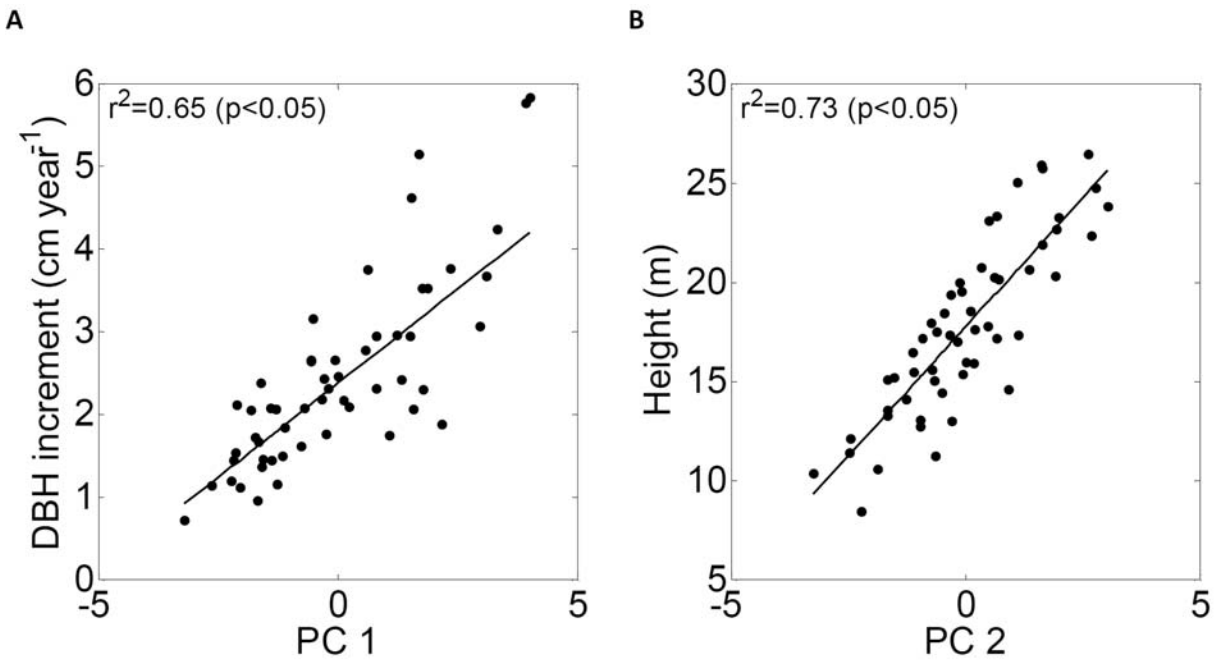

707

708

709 Figure 4: Relationship between field measured stand attributes and the first two principal components

710 derived from the wood fiber attributes. PC1 was strongest related to the annual increment in DBH (A),

711 PC2 was strongest related to the canopy height (B).

712

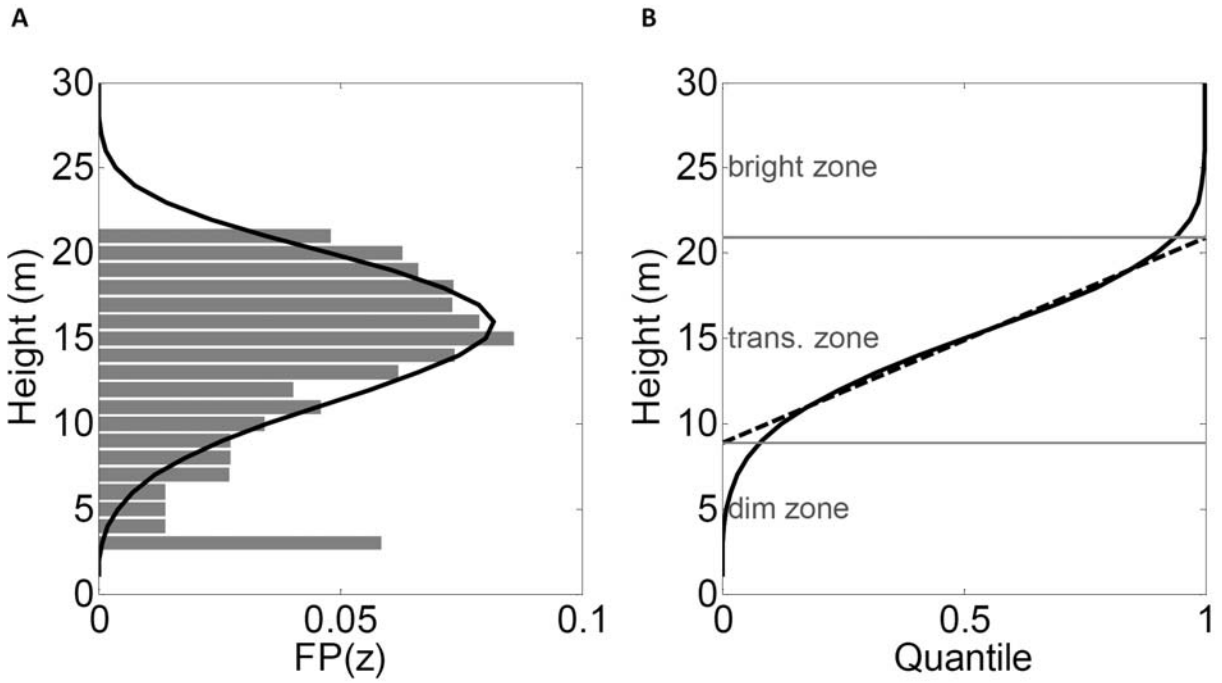

Figure 5: (a) Example of a canopy profile derived for one individual pixel of the LiDAR dataset (here using r=3832, c=4065 as an example). The observed foliage density profile is shown as gray bars and plotted in steps of one meter canopy height, the fitted Weibull curve is presented as black line. (b): Cummulative foliage density profile (same as in 5a) and fitted linear regression between 0.1 and 0.9 quantile. The slope and offset of the regression line define the bright, transition and dim canopy zone

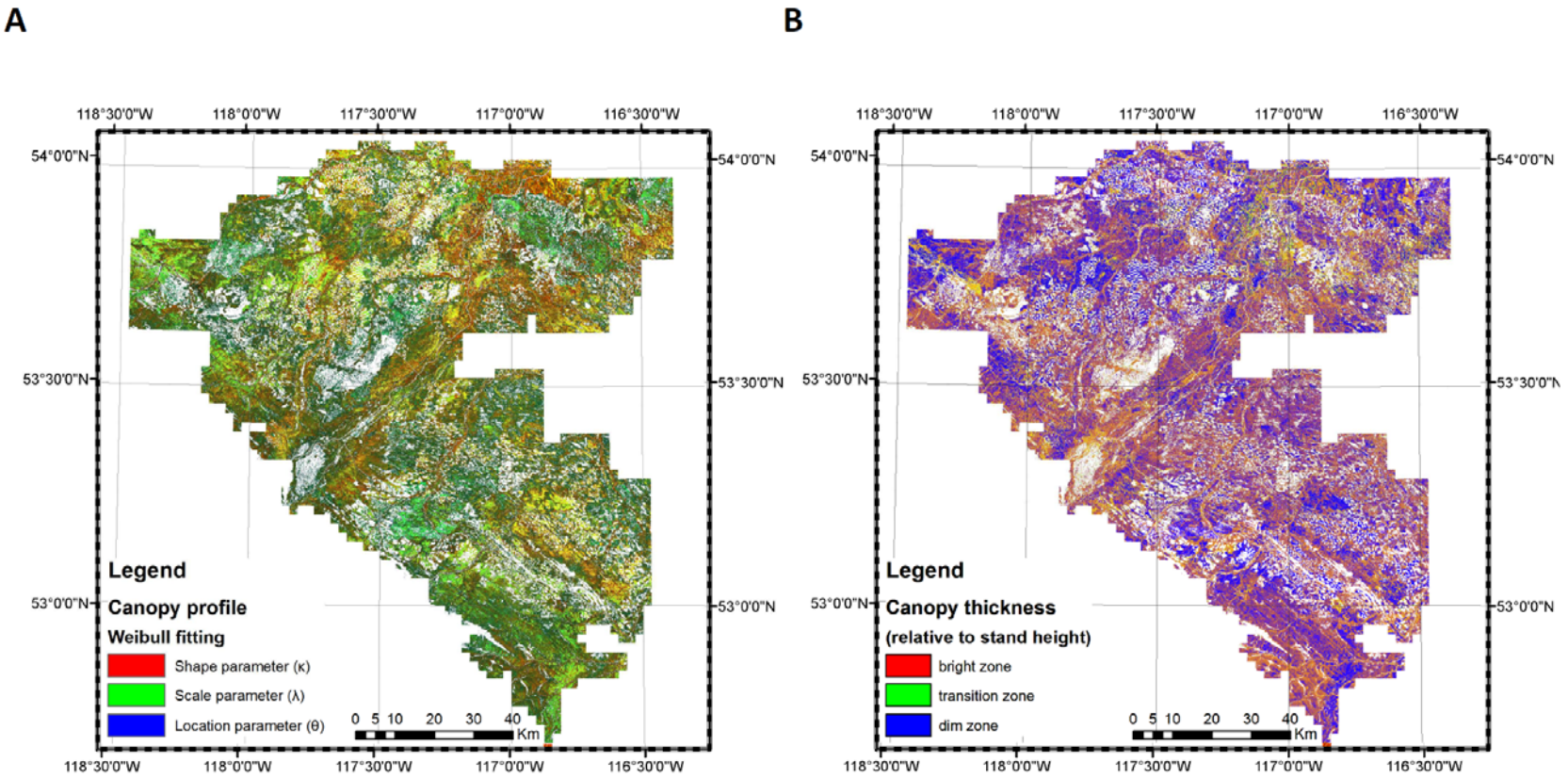

Figure 6: (a) Map of the Weibull coefficients (shape parameter, scale parameter and location parameter) across the entire LiDAR dataset. A Weibull curve was fitted to the profile observed for each individual pixel (10m x 10 m), analogous to Figure 5a. The mean value for the three Weibull coefficients was 4.62 (σ=6.23), 1.44(σ=2.33) and 0.13 (σ=0.22) (b): Canopy zones (bright, transition and dim) for the entire LiDAR dataset, derived analogous to Figure 5b. The thickness of the canopy zones ranged from 0-8.57 m, 0-26.54 m and 0-3.94 m for bright, transition and dim zone, respectively.

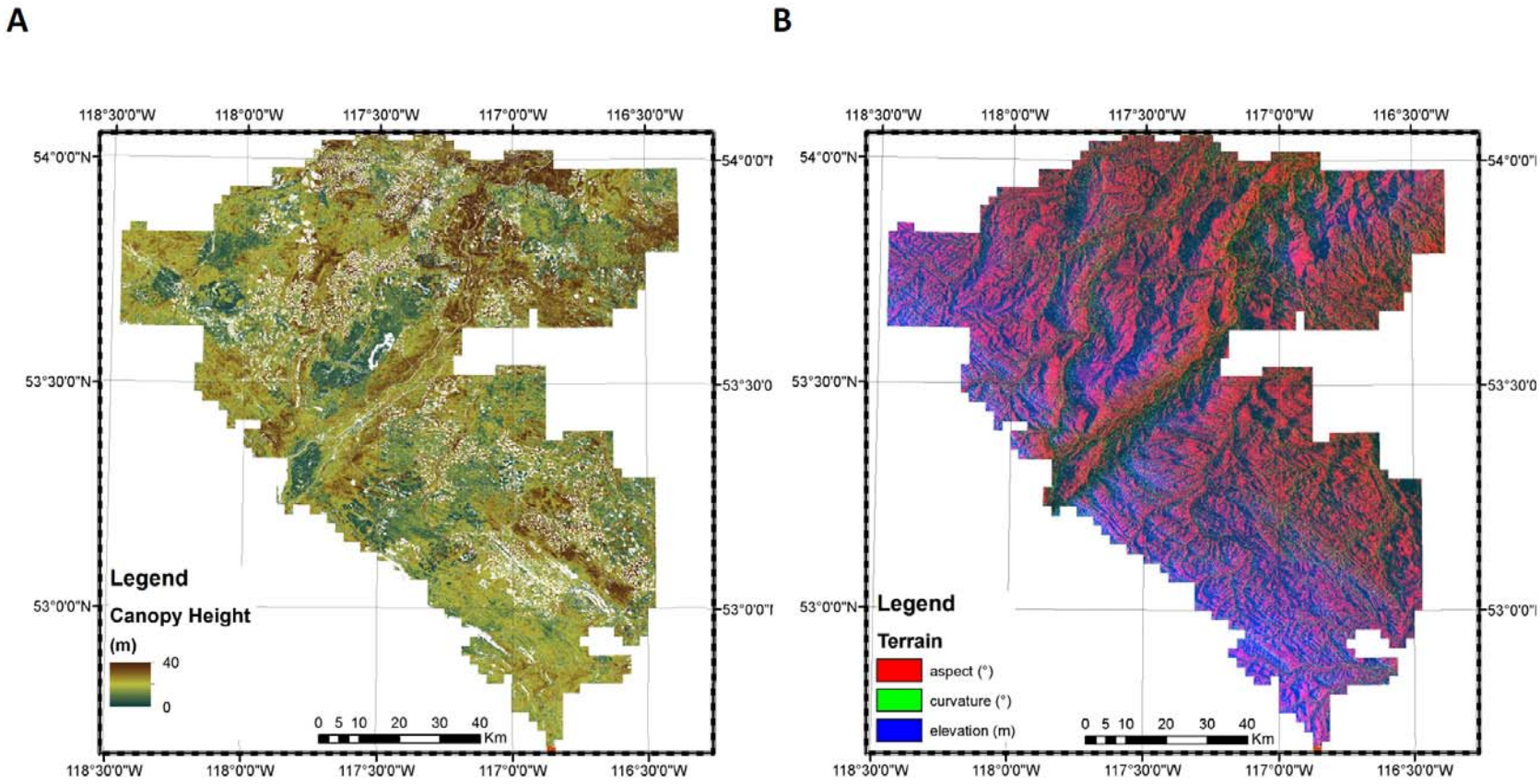

731

732

733 Figure 7: (a) Map of stand heights estimated from LiDAR (mean of the top 5% of the LiDAR returns); (b): Terrain aspect, curvature and elevation

734 derived from LiDAR. The mean elevation was 668.89 m (σ= 638.98m). Mean terrain curvature: 0.00^{o} (σ=0.01^{o}), mean aspect: 7.01^{o}, (σ=55.17^{o})

735

736

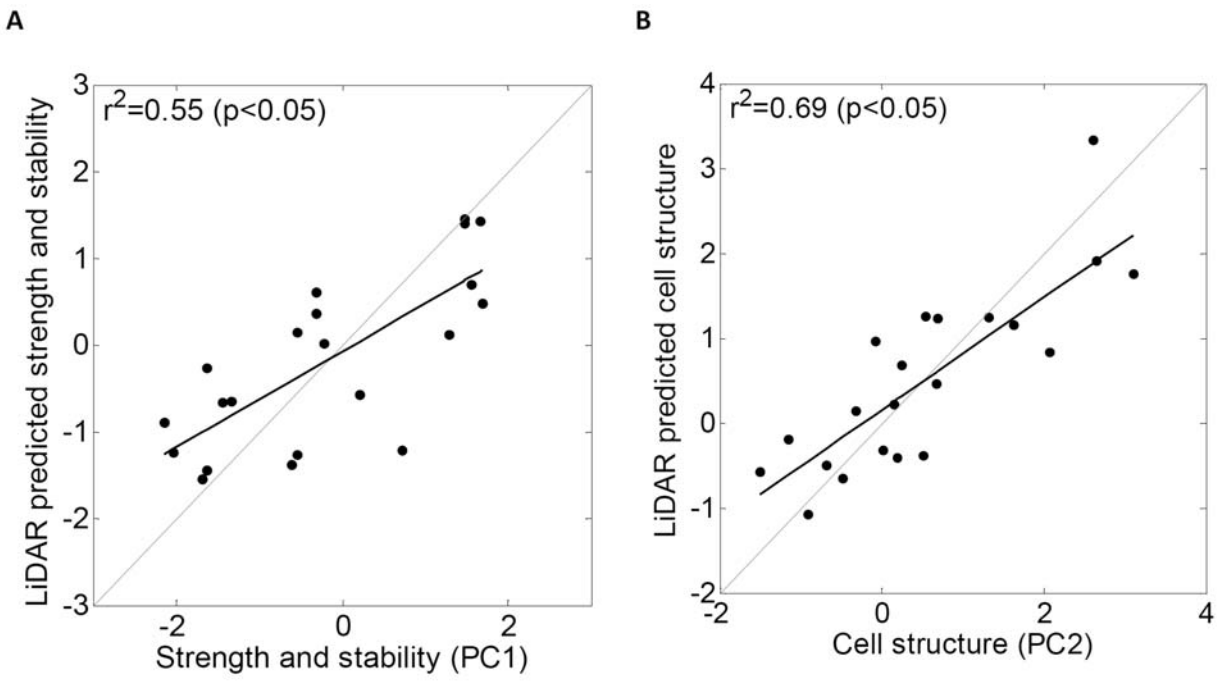

737

738

739 Figure 8: Relationship between field-measured LiDAR-observed stand attributes and the first two

740 principal components derived from the wood fiber attributes PC1 (A), PC2 (B).

741

742

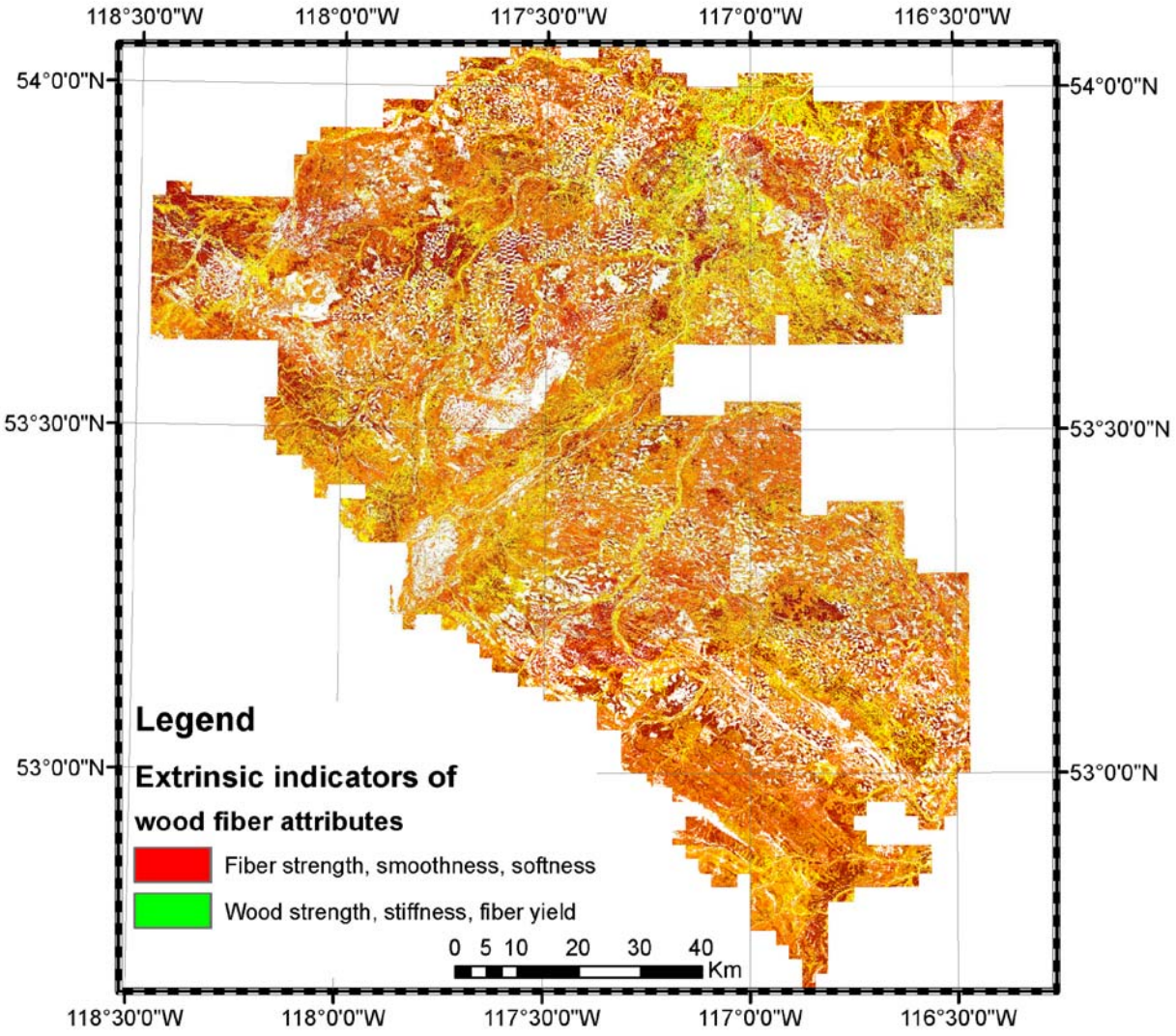

Figure 9: LiDAR derived model of the first two principal components of the wood fiber attributes across the entire study area. Harvested areas are excluded from this graph. The data range shown for PC1 is -3 to +3, the range shown for PC2 is -5 to +5.